

Impact of N, O Heteroatoms in Asphaltene on Adsorption of Vanadyl/Nickel Etioporphyrin

Feifei Chen, Qin Wang, Linzhou Zhang, and Qiushi Zhu*

Cite This: *ACS Omega* 2022, 7, 39078–39089

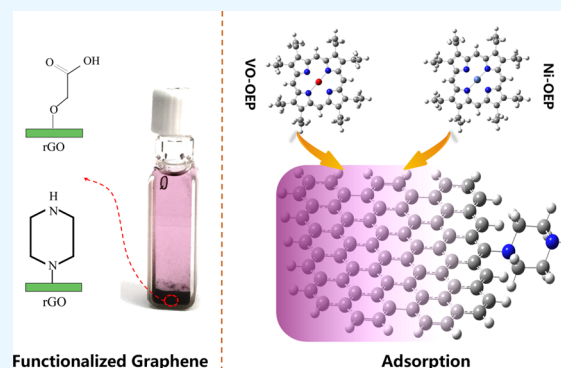
Read Online

ACCESS |

Metrics & More

Article Recommendations

ABSTRACT: The interaction between functionalized graphene and metal porphyrins was studied for a better understanding of the influence of the N and O heteroatoms in asphaltene on demetallization efficiency during the solvent deasphalting process. The theoretical simulation indicated a strong inhibitory effect of the aminated/carboxylated side group for chemical adsorption of metal porphyrins. The differences of adsorption behavior for graphene, aminated graphene, and Canadian oil sands bitumen vacuum tower bottom asphaltene (VTB-asp) were also analyzed. It was found that the introduction of aminated side groups to the graphene not only compromised the electron delocalization capacity of the polyaromatic nuclei hydrocarbon skeleton of graphene but also caused a steric hindrance effect on the internal diffusion of metal porphyrins, leading to decreased adsorption active sites and internal diffusion rate, respectively. It was also found that metal porphyrins can be barely adsorbed on carboxylated graphene at 25 °C.



1. INTRODUCTION

With the growing consumption of liquid petroleum products and the worsening deterioration of crude oil, low-quality oil processing becomes a new development trend of oil refining technology. The combination of technology with traditional processes such as the fluid catalytic cracking (FCC) process can effectively improve the utilization of inferior raw materials. However, heavy metals in heavy fractions of crude oil, such as nickel and vanadium, always destroy the crystal structure of the catalyst, leading to catalyst deactivation and a large amount of catalyst consumption.^{1–4} The majority of these metals are concentrated in both resin and asphaltene fractions of heavy oil. During the solvent deasphalting process, the resinous shell of asphaltene is unstable and quickly get aggregated in alkene solvents.⁵ Most of the heavy metals are physically/chemically captured and removed together with the de-oiled asphalt.^{5–10} However, the presence of trace metals in deasphalted oil (DAO) can still poison the FCC catalyst.¹¹ Filby and Strong¹² had found that about 23.1% of vanadium was observed in the DAO of the Athabasca bitumen and result in its poor processability for the FCC process. Therefore, it is crucial to investigate the interactions between metal and asphaltene to enhance the adsorption process and the demetallization efficiency of the solvent deasphalting process.

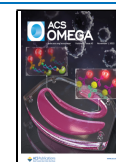
In general, asphaltene could interact with other materials through hydrogen bonding, dipole–dipole interactions, van der Waals forces, as well as ion-exchange interactions.^{13–18} Santos Silva⁸ confirmed that hydrogen bonding and lateral

chains played a vital role for the capture of metal porphyrins during asphaltene aggregation from the experimental and molecular dynamics simulation results. However, the petroleum asphaltene is a complex molecular mixture, and individual molecules have very complex structures. Schuler et al.^{19,20} have proved that most of the individual petroleum asphaltene molecules consist of a central aromatic core and long side alkane chains by combining atomic force microscopy and scanning tunneling microscopy analysis. It is hard to figure out which structure contribute to the adsorption of metal porphyrins. Proper model compounds with relatively simple structures may be a good and fast approximation to study their adsorptive properties.²¹ Several well-defined molecules, such as pyrene,²² hexabenzocoronene derivatives,²³ as well as Violanthrone-78, Violanthrone-79, and Xylenol Orange tetrasodium salt,²¹ were used as model compounds to study the associative properties of asphaltene. In previous studies,^{6,24,25} adsorption of vanadyl octaethylporphyrin (VO-OEP) and nickel octaethylporphyrin (Ni-OEP) on Canadian oil sands bitumen vacuum tower bottom asphaltene (VTB-asp) and

Received: July 29, 2022

Accepted: October 7, 2022

Published: October 19, 2022



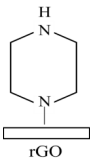
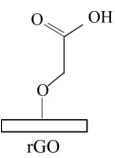
graphene was studied. The results showed that the aromatic core of asphaltene was the principal structure for the adsorption of metal porphyrins. We also hypothesized that the lateral chains and heteroatoms of asphaltene may bring in some adverse effects, as the adsorption uptake of metal porphyrins on graphene was more than that on asphaltene.

To validate the speculation, the adsorption property of N- or O-modified graphene was investigated in this study. As in asphaltene, N-containing heterocycles are the most prevalent forms of nitrogen,²⁶ while the majority of the oxygen are in the form of hydroxyl groups as well as carboxyl functions.²⁷ Graphene with N (modified with piperazine, aminated graphene) or O (modified with carboxyl, carboxylated graphene) containing groups were used as model compounds to verify the influence of the heteroatoms during adsorption of metal porphyrins in this study. Moreover, the heavy metal, especially for nickel and vanadium, always exist in the form of metal porphyrins in crude oil, which may have a great structural diversity.^{11,28} For simplicity, VO-OEP and Ni-OEP, which is structurally similar to the petroporphyrins, were used as substitutes for these porphyrins to investigate their interaction behaviors with asphaltene. Metal porphyrins' adsorption on the model compounds was carried out in *n*-pentane, with the same experimental conditions of the previous one.²⁵ Adsorption kinetics and thermodynamics were carried out, and the results were compared with some already reported data to evaluate the metal porphyrins' adsorption differences and similarities on different adsorbents.

2. EXPERIMENTAL AND THEORY

2.1. Materials. Aminated graphene and carboxylated graphene as well as graphene used in the experiment were purchased from Nanjing XFNANO Co., Ltd. The structure and properties are given in Table 1. The metal porphyrins, VO-

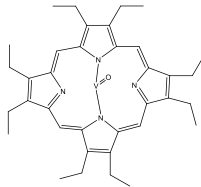
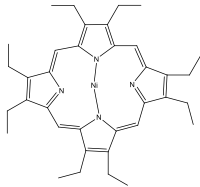
Table 1. Properties of Modified Graphene

property	aminated graphene	carboxylated graphene
content	about 8 wt.%	about 4 wt.%
structure		

OEP and Ni-OEP, were obtained from J&K Scientific Ltd. The specifications of them are shown in Table 2. Other chemical reagents, obtained from Anhui Longda Chemical Works, were of analytical grade and implemented without any further purification.

2.2. Adsorption Test. The standard curve of metal porphyrins: Because of the poor solubility of metal porphyrins in *n*-pentane,²⁹ an ultrasonic oscillating assisted method was used to avoid formation of incompletely solubilized porphyrin particles, which may cause inaccurate results. First, metal porphyrin was dissolved in toluene to obtain the stock solution with the concentration of 100 $\mu\text{g/mL}$. A definite amount of stock solution was pipetted into a series of 25 mL volumetric flask to remove toluene using the vacuum degassing method.

Table 2. Specifications of VO-OEP and Ni-OEP

property	vanadyl octaethylporphyrin	nickel octaethylporphyrin
structure		
molecular formula	$\text{C}_{36}\text{H}_{44}\text{N}_4\text{OV}$	$\text{C}_{36}\text{H}_{44}\text{N}_4\text{Ni}$
color	red to purple	red to purple
molecular weight	599.71	591.45

The residue was redissolved in *n*-pentane with ultrasonic oscillation to prepare the standard work solution, in which the metal porphyrin was 1, 2, 4, 6, 8, 12, and 16 $\mu\text{g/mL}$, respectively. Then, the UV–visible absorption of the work solution were measured. The absorbance of Ni-OEP at 550 nm and VO-OEP at 570 nm was plotted against its concentration to obtain the standard curve (Figure 1). The adjusted *R*-square of the standard curves was 0.9999 and 0.9987 for Ni-OEP and VO-OEP, respectively, which confirmed the excellent linearity of these curves.

Adsorption kinetic/thermodynamic:^{24,25} Adsorption kinetic/thermodynamic tests were carried out in a 1 cm path length, 5 mL quartz cuvette with a screw cap seal. A certain amount of aminated graphene and 3.5 mL metal porphyrin standard solution were added into the quartz cuvette at a certain temperature controlled using a constant temperature water bath oscillator. For the adsorption kinetic test, the absorbance of the solution at 550/570 nm was detected in regular periods of time, while it was detected after the adsorption reached equilibrium in the adsorption thermodynamic test. Then, the adsorption capacity (q_t , $\mu\text{g/g}$) and equilibrium adsorption capacity (q_e , $\mu\text{g/g}$) could be calculated by eq 1.

$$q_t = \frac{(c_1 - c_2)V}{M} \quad (1)$$

where c_1 is the initial concentration of the metal porphyrin ($\mu\text{g/mL}$), c_2 is the concentration of the metal porphyrin at a given time t , V is the solution volume (mL), and M is the aminated graphene dosage (g).

The adsorbent dosage, initial porphyrin concentration, and adsorption temperature were varied to investigate their impact on the adsorption of metal porphyrin. The detailed parameters for the adsorption kinetic/thermodynamic test are shown in Table 3.

2.3. Adsorption Kinetic and Thermodynamic Equations. The adsorption kinetics is significant for an adsorption process as it illustrates the controlling mechanism of the adsorption process (chemical reaction, diffusion, and mass transfer process). The kinetics results were analyzed by the pseudo-first-order,³⁰ pseudo-second-order,³¹ Elovich,³² and diffusion kinetic models³³ (Table 4). The pseudo-first-order equation and pseudo-second order equation are common kinetic models for describing a solid–liquid adsorption system. The Elovich equation refers to describe chemical adsorption,

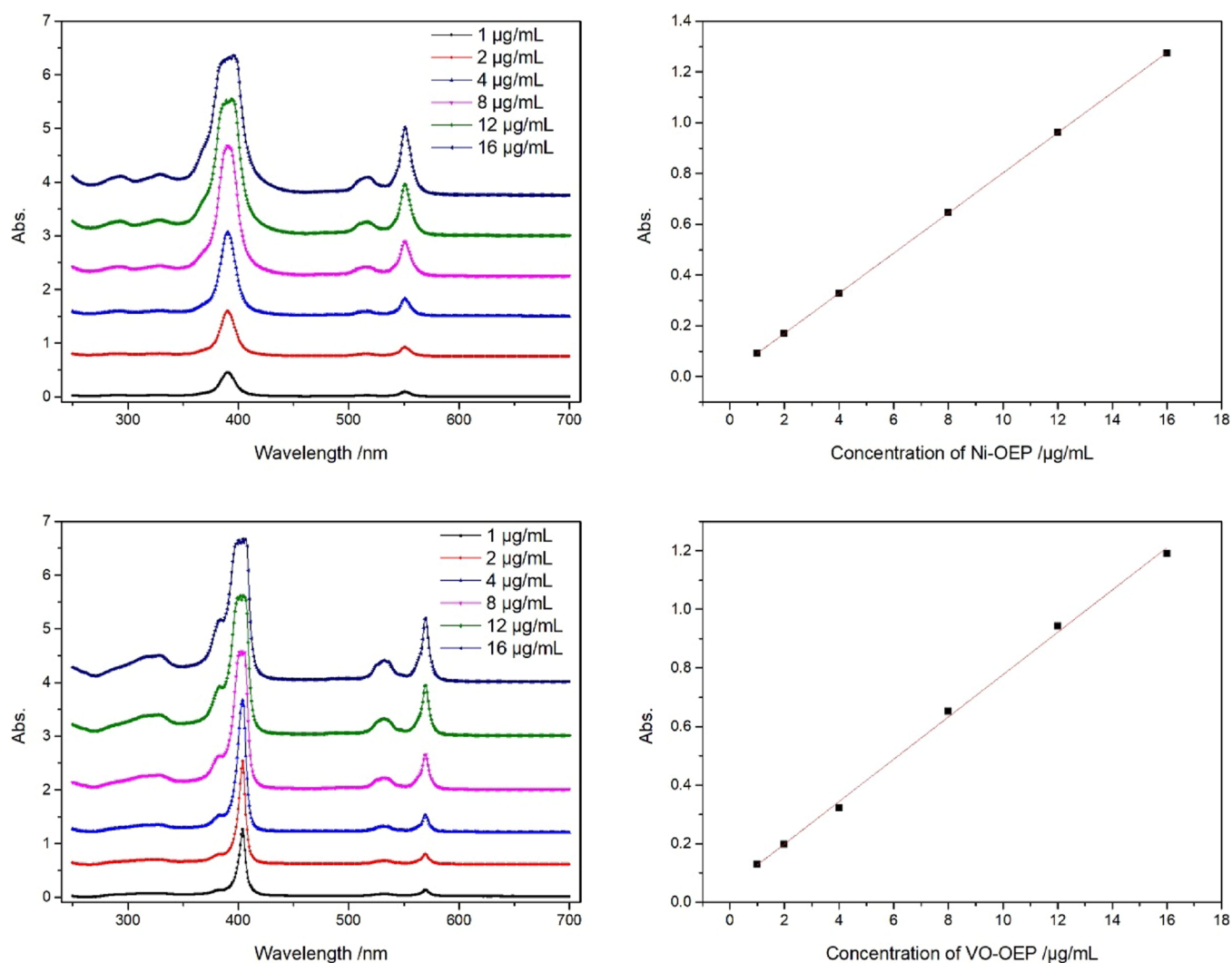


Figure 1. Standard curve of metal porphyrins.

Table 3. Initial Parameters for Adsorption Kinetics and Thermodynamic

adsorption	T °C	constant parameter	varied parameter
kinetic test	15, 20, 25 ^a °C	$m = 5$ mg $c = 10$ µg/mL	$c = 6, 10, 15$ µg/mL $m = 2, 5, 8$ mg
thermodynamic test	15, 20, 25 °C	$m = 10$ mg	$c = 6, 8, 10, 12, 14$ µg/mL

^aFor adsorbent dosage and initial porphyrin concentration tests, the temperature was 25 °C.

and the diffusion kinetic model is used to describe both the pore and surface diffusion. The thermodynamic results were adjusted by the Langmuir and Freundlich isotherm equations.³⁴ Thermodynamic parameters including ΔG° , ΔH° , and ΔS° were calculated.³⁵

2.4. Analytical Methods. The UV-1601 ultraviolet visible spectrophotometer, from the Beijing Beifen-Ruili Analytical Instrument Co., Ltd., was used for the quantitative analysis of metal porphyrins. The HX-101 constant temperature water bath oscillator, from the Beijing Changliu Scientific Instrument Co., Ltd. with a temperature range of -15 to 95 °C and the precision of temperature control of ± 0.1 °C, was used for holding the adsorption temperature at a suitable temperature.

TEM micrographs of aminated graphene were obtained using JEM-2100 URP TEM of Jeol Ltd. The acceleration voltage was 80–200 kV. The point resolution is 0.19 nm and

the linear resolution is 0.14 nm. The range of element resolution is B5~Pu94. XPS was tested by Escalab 250Xi XPS of Thermo Fisher Scientific. The excitation resource is Al Ka. The ion source is 100 eV–4 keV.

3. RESULTS AND DISCUSSION

3.1. Characterization of Aminated Graphene. The TEM micrographs of graphene and modified graphene before and after the thermodynamics tests at 20 °C are shown in Figure 2. The results revealed a change in the surface morphology of aminated graphene after the adsorption of the metal porphyrins. The clear, layered, and transparent image is covered with small and closely spaced dots after adsorption of VO-OEP, while it is covered with broad irregular black spots after the adsorption of Ni-OEP. Dots and spots resultant from the aggregation of metal porphyrins confirmed the adsorption

Table 4. Adsorption Kinetic and Thermodynamic Equations^a

name	equation
pseudo-first order equation	$q_t = q_e (1 - e^{-k_1 t})$ (2)
pseudo-second order equation	$q_t = k_2 q_e^2 t / (1 + k_2 q_e t)$ (3)
Elovich equation	$q_t = \ln(AB)/B + \ln(t)/B$ (4)
diffusion equation	$q_t = k_p t^{0.5} + C$ (5)
Langmuir adsorption isotherm	$\frac{C_e}{q_e} = \frac{1}{q_{L_{\max}}} \frac{C_e}{q_{\max}}$ (6)
Freundlich adsorption isotherm	$\log q_e = \frac{1}{n} \log C_e + \log K_F$ (7)
adsorption thermodynamic	$\Delta G^\circ = \Delta H^\circ - T \Delta S^\circ$ (8)
	$\Delta G^\circ = -RT \ln K$ (9)
	$\ln K = \frac{\Delta S^\circ}{R} - \frac{\Delta H^\circ}{RT}$ (10)

^a q_e and q_t : the adsorption capacity ($\mu\text{g/g}$) at equilibrium and at time t ; k_1 , k_2 , and k_p : the rate constant of adsorption (min^{-1}); A , B , and C : constants; C_e : the equilibrium concentration ($\mu\text{g/mL}$); K_L : the Langmuir constant (L/mg); K_F and $1/n$: the Freundlich constants; R : the universal gas constant ($8.314 \text{ J}\cdot\text{mol}^{-1}\cdot\text{K}^{-1}$); T : adsorption temperature (K).

processes. However, when compared with the graphene images, it can be found that these dots and spots are little looser. In adsorption tests shown in the latter part of the study, it can also be found that the equilibrium adsorption capacity of metal porphyrins decreased significantly, when aminated graphene was used as the adsorbent under the same experimental conditions. It can be deduced that the introduction of the aminated group to the hydrocarbon skeleton reduced the interaction between adsorbent and metal porphyrins. However, there is no significant difference among TEM micrographs of carboxylated graphene, which indicated that metal porphyrins are hardly adsorbed on the carboxylated graphene. The unchanged micrographs also confirmed that metal porphyrins were adsorbed rather than just deposited on the adsorbents.

As metal porphyrins interacted with the surface of aminated graphene through various interaction forces, XPS spectra of aminated graphene before and after adsorption of metal porphyrins were also analyzed to verify the adsorption of metal porphyrins. The results were presented in Figure 3. The V 2p peak at 516.4 eV and the Ni 2p peak at 853.9 eV of aminated graphene clearly illustrated that metal porphyrins were adsorbed on aminated graphene, which is in accordance with the TEM results.

3.2. Adsorption Kinetics. Adsorption of metal porphyrins was studied by adsorption kinetics tests. Evolution of

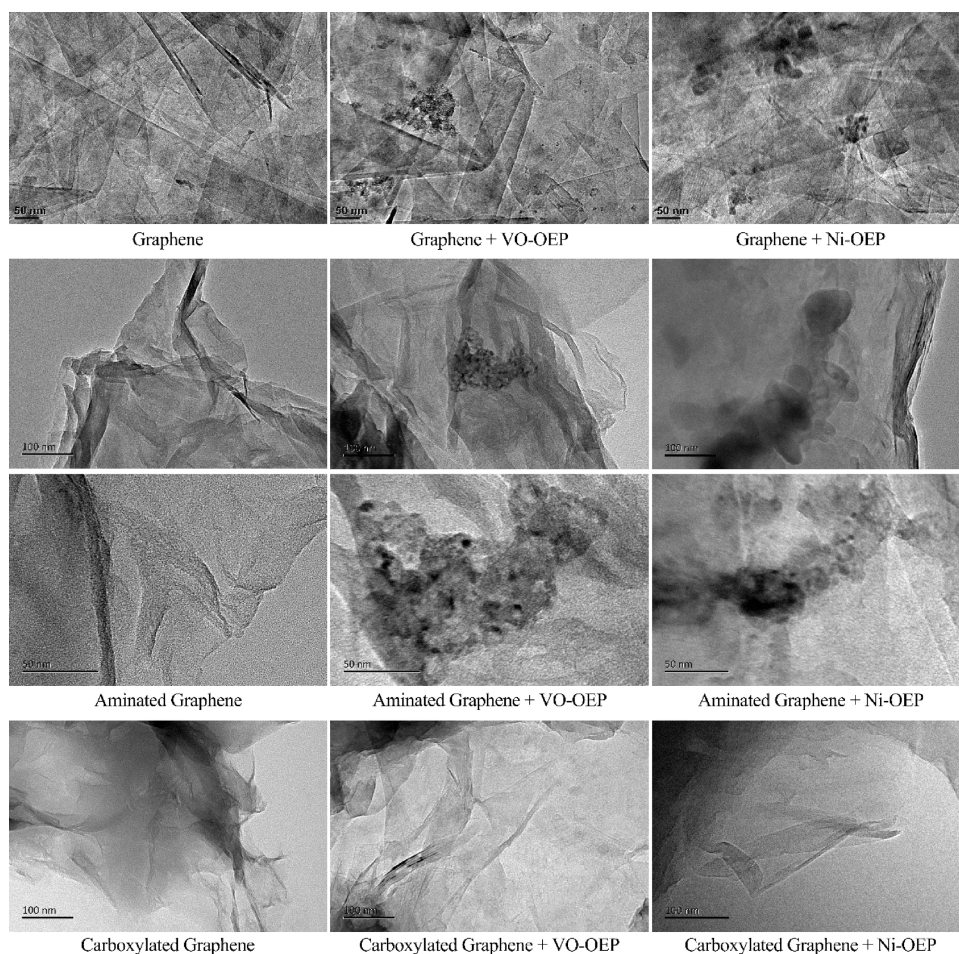


Figure 2. TEM images of graphene and modified graphenes for the adsorption of metal porphyrins. TEM images of graphene are reused (Reprinted in part with permission from Chen et al.²⁵ Copyright 2018 Elsevier B.V.)

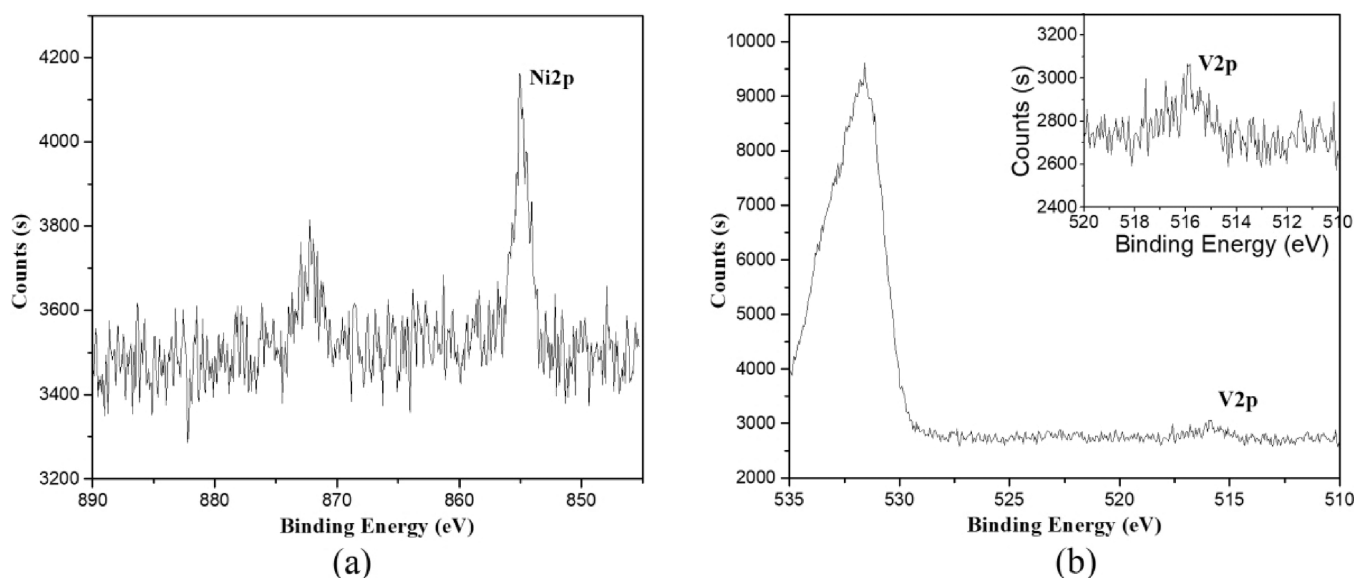


Figure 3. XPS spectra of aminated graphene before and after adsorption: (a) Ni (2p) (853.9 eV), aminated graphene + Ni-OEP; (b) V (2p) (516.4 eV), aminated graphene + VO-OEP.

adsorption capacity with time corresponding to different experimental conditions, such as adsorption temperature, initial metal porphyrin concentration, and adsorbent dosage were studied carefully. The experimental data were simulated by four types of adsorption kinetic models for investigating the rate-controlling step of adsorption.

The influence of adsorption temperature on metal porphyrins' adsorption was studied at 15, 20, and 25 °C, while the aminated graphene was 0.0050 g and the initial porphyrin concentration was 10 $\mu\text{g/mL}$. Evolution of porphyrins' adsorption capacity with time are shown in Figure 4a. As the temperature increased from 15 to 25 °C, the equilibrium adsorption capacity decreased from 1092 to 904 $\mu\text{g/g}$ for VO-OEP and from 912 to 684 $\mu\text{g/g}$ for Ni-OEP, which indicated an exothermic process for the adsorption of metal porphyrins. The results were adequately fitted by the pseudo-first-order equation with the correlation coefficients (R^2) between 0.995 and 0.999 (Figure 4a and Table 5). The experimental equilibrium adsorption capacity ($q_{\text{e exp}}$) was in accordance with that calculated by the pseudo-first-order equation ($q_{\text{e cal}}$). Figure 4 also indicated that the adsorption process consists of three consecutive steps: fast adsorption step ($t < 30$ min), slow adsorption step ($30 \text{ min} < t < 150$ min), and equilibrium step ($t > 150$ min). It may be deduced that the adsorption of metal porphyrins was affected by the number of free adsorption sites.³⁶

For carboxylated graphene, adsorption temperature makes a similar impact on metal porphyrins' adsorption (Figure 5). At 25 °C, metal porphyrins, VO-OEP or Ni-OEP, can barely be adsorbed on carboxylated graphene, which means that the adverse impact of the carboxyl group on adsorption is greater than that of piperazine. Therefore, no further investigation of the influence of initial porphyrin concentration and adsorbent dosage with carboxylated graphene was ever taken.

However, the influence of initial porphyrin concentration on adsorption with aminated graphene has been studied. As illustrated in Figure 4b, when the initial porphyrin concentration was increased from 6 to 15 $\mu\text{g/mL}$, the uptake of VO-OEP and Ni-OEP at equilibrium increased from 690 to 944 $\mu\text{g/g}$ and from 592 to 742 $\mu\text{g/g}$, respectively. The results

indicated that higher initial porphyrin concentration favored the diffusion of porphyrins from solution to the surface of the adsorbent and facilitated the adsorption of metal porphyrins to the active sites. The results were also well fitted by the pseudo-first-order equation with a relative error of $q_{\text{e exp}}$ and $q_{\text{e cal}}$ lower than 1% (Table 6). As the initial porphyrin concentration increased, the rate constant (k_i) decreased, which may be attributed to the increased collisions of metal porphyrins.^{24,25}

Uptake of VO-OEP and Ni-OEP at equilibrium was also affected by the dosage of aminated graphene. When the adsorbent increased from 2 to 8 mg, the uptake of VO-OEP and Ni-OEP at equilibrium decreased from 1108 to 839 $\mu\text{g/g}$ and from 814 to 573 $\mu\text{g/g}$, respectively (Figure 4c). The rate constant (k_i) increased with the dosage of aminated graphene. The interfacial area increased with the adsorbent dosage and therefore resulted in more available combining sites and increased k_i .

3.3. Adsorption Isotherms and Thermodynamics.

Adsorption thermodynamics were investigated at 15, 20, and 25 °C with constant adsorbent dosage and varied initial porphyrin concentration. The experimental data were fitted with Langmuir and Freundlich isotherm equations, and the results were presented in Figure 6 and Table 7. The experimental data could be well fitted by the Langmuir isotherm equation with regression coefficients nearly equal to 1. The adsorption could be considered as the monolayer adsorption. The results also showed that the fitting parameters, K_L and $q_{\text{max}} \cdot K_L$, decreased with the increase in temperature. Therefore, the aminated graphene showed a higher affinity with metal porphyrins at lower temperatures. A decrease in adsorption temperature will increase the equilibrium adsorption capacity of the metal porphyrins, which was already discussed in the adsorption kinetics study. In addition, the K_L and $q_{\text{max}} \cdot K_L$ for the adsorption of VO-OEP were higher than those of Ni-OEP. It means that the removal of VO-OEP by adsorption was easier than Ni-OEP.

According to the Van't Hoff equation, the thermodynamic parameters of the adsorption including ΔG° , ΔH° , and ΔS° were calculated and shown in Table 8 by plotting $\ln K_L$ versus $1/T$ (Figure 7). Adsorption of metal porphyrins onto aminated

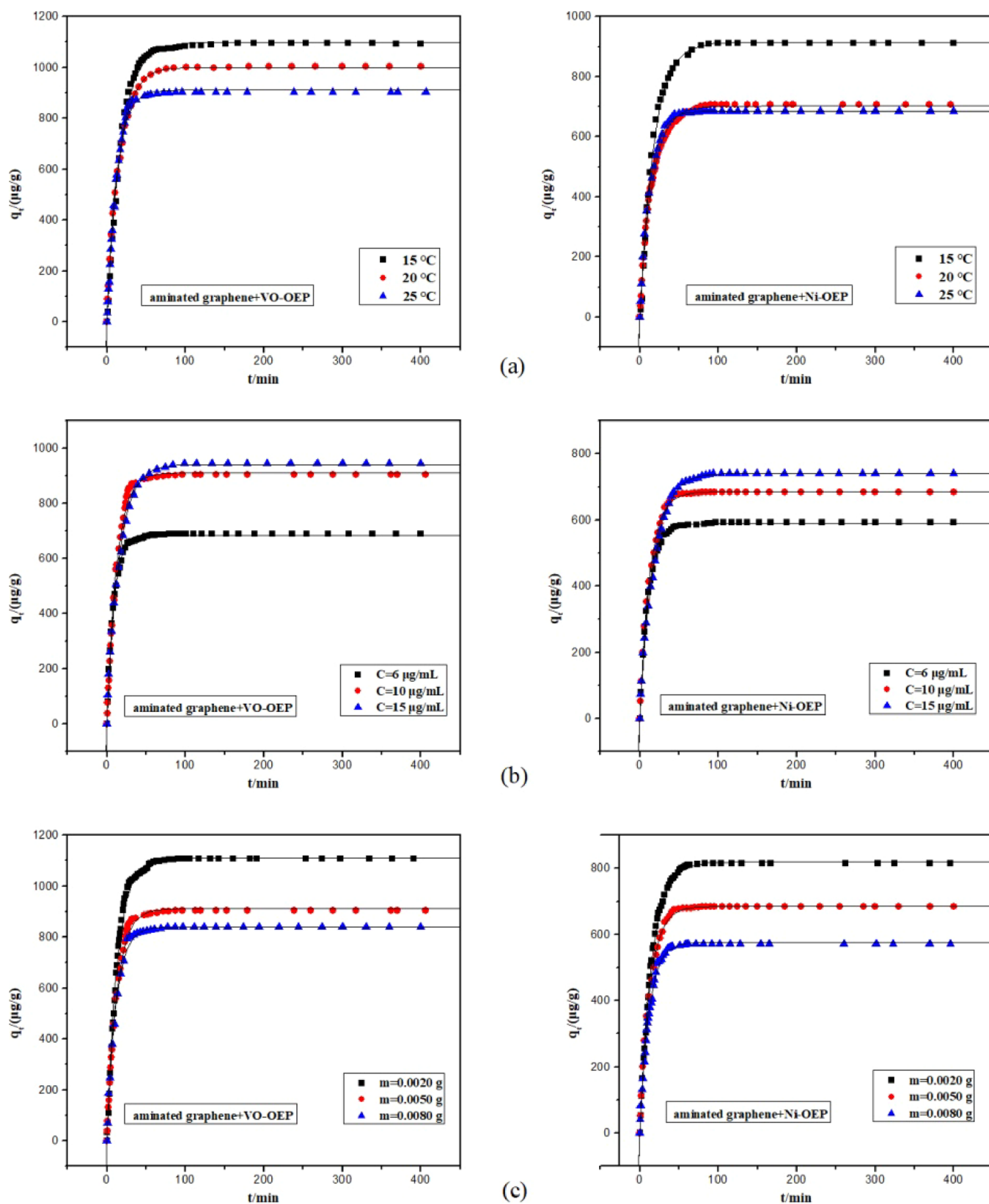


Figure 4. Evolution of adsorption capacity of aminated graphene with time at different temperatures (a), initial metal porphyrin concentrations (b), and aminated graphene dosages (c). Solid lines represent pseudo-first-order results.

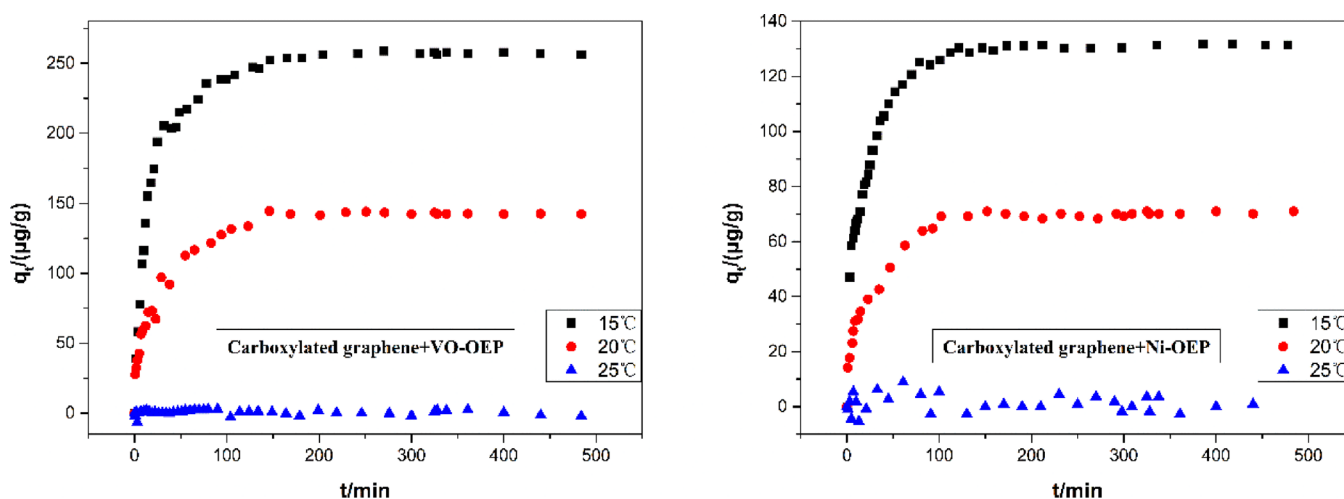
graphene is confirmed to be a spontaneous, exothermic process ($\Delta G^\circ < 0$, $\Delta H^\circ < 0$), which means that low temperature favored the promotion of the removal efficiency of the metal porphyrins. Therefore, the thermodynamics study was in

accordance with the kinetic one. As already discussed in our previous study,^{24,25} the ΔG° of chemical adsorption, with the formation of the covalent bond, is about -400 to -80 $\text{kJ}\cdot\text{mol}^{-1}$, while the ΔG° of physical adsorption is about -20 to 0

Table 5. Kinetic Parameters Calculated Using Four Kinetic Models for the Adsorption of Porphyrins on Aminated Graphene at Different Temperatures^a

sample	<i>T</i> (°C)	pseudo-first-order equation				pseudo-second-order equation				<i>q_e</i> exp (μg/g)
		<i>q_e</i> cal (μg/g)	<i>k₁</i> (min ^{−1})	<i>R</i> ²	<i>δ</i>	<i>q_e</i> cal (μg/g)	<i>k₂</i> (μg·μg ^{−1} ·min ^{−1})	<i>R</i> ²		
VO-OEP	15	1099	0.0561	0.996	0.006	1213	66.5	0.959		1092
	20	1000	0.0638	0.999	0.002	1081	88.3	0.984		1002
	25	911	0.0801	0.996	0.008	988	119.5	0.958		904
Ni-OEP	15	915	0.0554	0.995	0.003	1005	75.4	0.966		912
	20	702	0.0634	0.998	0.008	775	117.4	0.981		708
	25	685	0.0782	0.999	0.001	735	174.3	0.974		684

sample	<i>T</i> (°C)	Elovich equation			diffusion equation		
		<i>B</i> (mg/μg)	<i>A</i> (μg·g ^{−1} ·min ^{−1})	<i>R</i> ²	<i>C</i> (μg/g)	<i>k_p</i> (μg/(g·min ^{0.5}))	<i>R</i> ²
VO-OEP	15	4.94	346	0.847	488	46.9	0.516
	20	5.93	419	0.895	418	42.1	0.587
	25	6.61	501	0.831	422	36.7	0.478
Ni-OEP	15	5.83	235	0.874	347	41.3	0.587
	20	7.88	272	0.877	328	30.1	0.549
	25	9.51	563	0.839	366	24.7	0.463

^a*δ*: relative error, $\delta = (q_{e\text{ cal}} - q_{e\text{ exp}})/q_{e\text{ exp}}$ **Figure 5.** Evolution of the adsorption capacity of carboxylated graphene with time at different temperatures.**Table 6. Pseudo-First-Order Kinetic Parameters for the Adsorption of Porphyrins on Aminated Graphene at Different Initial Concentrations and Dosages^a**

initial concentrations <i>T</i> = 25 °C, <i>m</i> = 5 mg		pseudo-first-order equation					<i>q_e</i> exp (μg/g)
	<i>C₀</i> (μg/mL)	<i>q_e</i> cal (μg/g)	<i>k₁</i> (min ^{−1})	<i>R</i> ²	<i>δ</i>		
VO-OEP	6	685	0.118	0.995	0.008		690
	10	911	0.0801	0.996	0.008		904
	15	941	0.0653	0.995	0.003		944
Ni-OEP	6	589	0.0914	0.997	0.010		592
	10	685	0.0782	0.999	0.001		684
	15	742	0.0561	0.996	0.0005		742

dosages <i>T</i> = 25 °C, <i>C</i> = 10 μg/mL		pseudo-first-order equation					<i>q_e</i> exp (μg/g)
	<i>m</i> (mg)	<i>q_e</i> cal (μg/g)	<i>k₁</i> (min ^{−1})	<i>R</i> ²	<i>δ</i>		
VO-OEP	2	1110	0.0748	0.996	0.002		1108
	5	911	0.0801	0.996	0.008		904
	8	840	0.0871	0.996	0.001		839
Ni-OEP	2	819	0.0659	0.999	0.006		814
	5	685	0.0782	0.999	0.001		684
	8	577	0.0845	0.996	0.006		573

^a*δ*: relative error, $\delta = (q_{e\text{ cal}} - q_{e\text{ exp}})/q_{e\text{ exp}}$

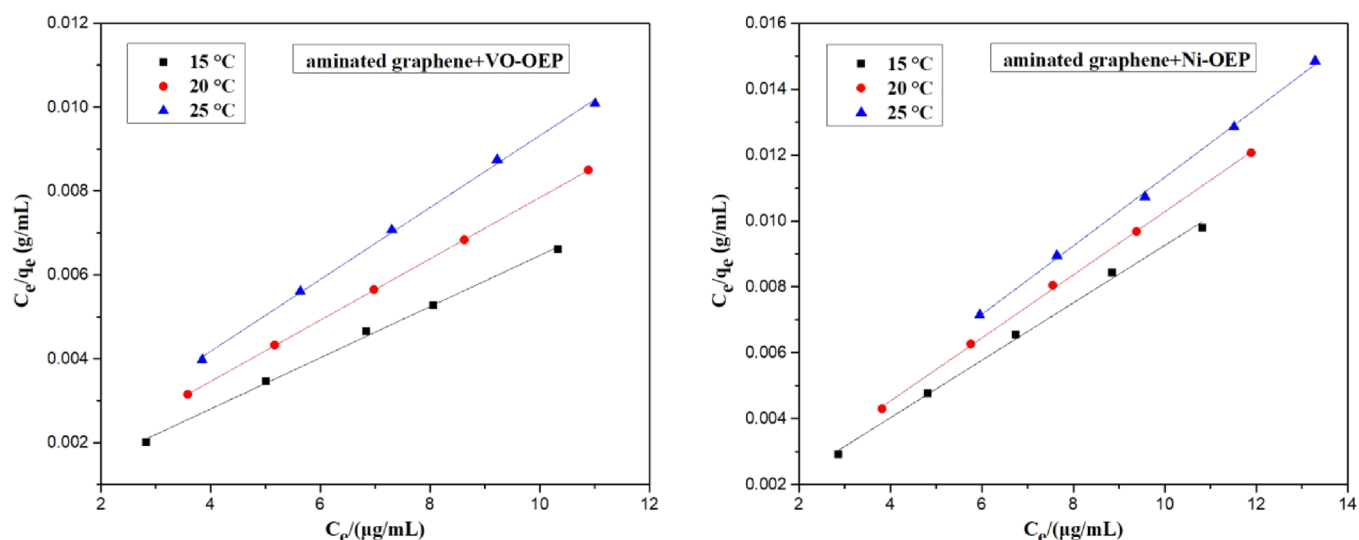


Figure 6. Langmuir isotherms.

Table 7. Isotherm Parameters and Correlation Coefficients

sample	<i>T</i> (°C)	Langmuir isotherm				Freundlich isotherm		
		<i>q</i> _{max} (μg/g)	<i>K</i> _L (mL/μg)	<i>q</i> _{max} · <i>K</i> _L (mL g ^{−1})	<i>R</i> ²	<i>K</i> _F	1/ <i>n</i>	<i>R</i> ²
VO-OEP	15	1639	1.69	2771	0.997	1282	0.081	0.883
	20	1368	1.38	1881	0.999	1000	0.107	0.981
	25	1166	1.15	1342	0.998	833	0.109	0.980
Ni-OEP	15	1147	1.60	1840	0.996	894	0.080	0.855
	20	1044	1.36	1418	0.999	784	0.093	0.984
	25	961	1.13	1087	0.998	702	0.098	0.855

Table 8. Adsorption Thermodynamic Results with Different Adsorbents

adsorbent	adsorbate	ΔG° (kJ/mol)			ΔH° (kJ/mol)	ΔS° (kJ/mol)
		288 K	293 K	298 K		
aminated graphene	VO-OEP	−1.258	−0.777	−0.347	−27.48	−91.1
	Ni-OEP	−1.131	−0.745	−0.305	−24.91	−82.5
graphene ²⁵	VO-OEP	−5.11	−4.27	−3.22	−59.54	−188.9
	Ni-OEP	−4.56	−3.70	−2.75	−56.73	−181.1
VTB-as ²⁴	VO-OEP	−16.54	−15.78	−15.21	−54.91	−133.3
	Ni-OEP	−15.40	−14.96	−14.26	−48.13	−113.5

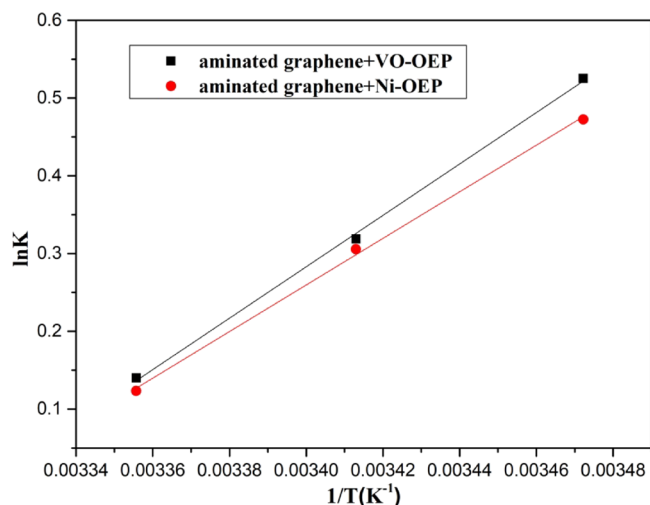


Figure 7. Van't Hoff plots of aminated graphene–porphyrins.

kJ·mol^{−1}, which is 5% of covalent bond strengths. As shown in Table 8, the ΔG° of the adsorption process confirmed a weak physical interaction between metal porphyrins and adsorbents. Schuler et al.³⁷ also found that physically combined asphaltene molecules formed nanoaggregates, and the ΔG° of the aggregation is ~ 20 kJ·mol^{−1}, which is in accordance with our findings.

3.4. Theoretical Simulation. Interactions between adsorbents (graphene and aminated graphene) and metal porphyrins were simulated, not only by Gaussian 09 in view of chemical adsorption, but also by Material Studio 8.0 in view of physical adsorption, to investigate the adsorption process.

Firstly, the full geometry optimizations of graphene, aminated graphene, VO-OEP and Ni-OEP were carried out at the B3LYP/6-31g* and LAN2DZ levels of theory. The results were shown in Figure 8. Then, the binding energy for each adsorption process was calculated by eq 11.

$$E_B = E_{ab} - (E_a + E_b) \quad (11)$$

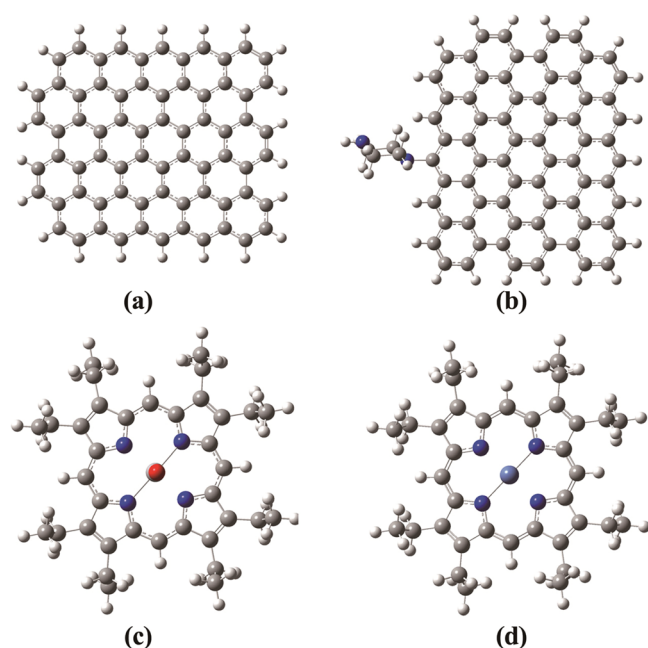


Figure 8. Optimized geometric structures: (a) graphene; (b) aminated graphene; (c) VO-OEP; (d) Ni-OEP.

where E_B is the binding energy, E_{ab} is the energy of the final optimized configuration, E_a and E_b are the energy of the adsorbent and the adsorbate, respectively.

The calculation results are shown in Table 9. The negative binding energy indicated that chemical adsorption may occur.

Table 9. Binding Energy and Adsorption Loading of the Four Adsorption Processes

process	E_B (eV)	adsorption loading (per cell)
graphene + VO-OEP	−0.458	149
aminated graphene + VO-OEP	−0.012	142
graphene + Ni-OEP	−0.114	166
aminated graphene + Ni-OEP	−0.016	161

However, the binding energy showed a significant decline after the introduction of the aminated side group to the graphene. It indicated that chemical adsorption of metal porphyrins was

seriously inhibited by introducing aminated/carboxylated side groups, which will lead to an enormous decrease in adsorption capacity. The calculation results are in accordance with the experimental results (Table 10).

In the Material Studio 8.0 program, the 3D models of graphene and aminated graphene have been built and optimized ($a = 29.514 \text{ \AA}$, $b = 34.080 \text{ \AA}$, $c = 80.000 \text{ \AA}$, $\alpha = 90$, $\beta = 90$, $\gamma = 90$) (Figure 9). The Sorption Module and the

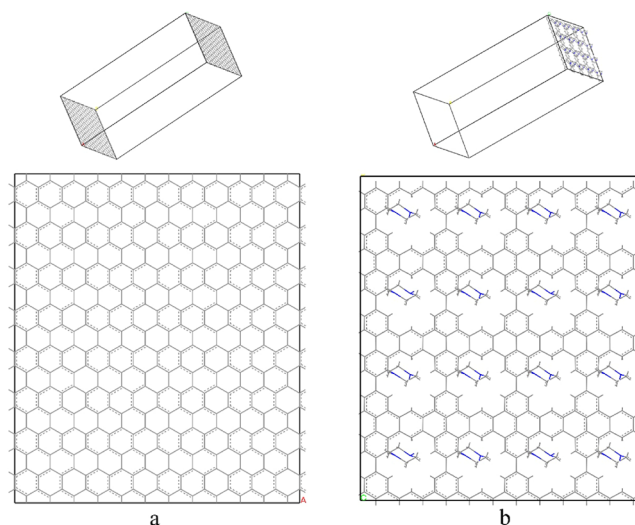


Figure 9. Optimized geometric structure in Material Studio 8.0 program: (a) graphene; (b) aminated graphene.

Universal Forcefield were then implemented for the simulation of the four adsorption processes. One lakh fifty thousand steps of equilibration steps and 35,000,000 steps of production steps were applied at 293 K and 100 kPa, respectively. After equilibrium, adsorption loading of the metal porphyrins was calculated and shown in Table 9. It can also be found that the adsorption loading of metal porphyrins reduced after the introduction of the aminated side group. However, the decline is relatively not evident. That is, the influence of the introduction on the physical adsorption of metal porphyrins is not noticeable. Actually, experimental results showed that the equilibrium uptake of metal porphyrins was drastically declined after the introduction. Combined with the discussion

Table 10. Adsorption Kinetics Results with Different Adsorbents^a

process	adsorption kinetics results					
aminated graphene	pseudo-first-order equation $q_t = q_e(1 - e^{-k_1t})$					
	$q_{e \text{ cal}}$ (mg/g)	k_1 (min ⁻¹)	R^2	$q_{e \text{ exp}}$ (mg/g)	equilibrium time (min)	
	VO-OEP	1.10	0.0561	0.996	1.09	150
	Ni-OEP	0.92	0.0554	0.995	0.91	150
graphene ²⁵	pseudo-second order equation $q_t = k_2q_e^2/(1 + k_2q_e t)$					
	$q_{e \text{ cal}}$ (mg/g)	k_2 (g·mg ⁻¹ ·min ⁻¹)	R^2	$q_{e \text{ exp}}$ (mg/g)	equilibrium time (min)	
	VO-OEP	6.70	0.0138	0.977	6.61	300
	Ni-OEP	6.67	0.0103	0.981	6.52	300
VTB-asp	pseudo-first-order equation $q_t = q_e(1 - e^{-k_1t})$					
	$q_{e \text{ cal}}$ (mg/g)	k_1 (min ⁻¹)	R^2	$q_{e \text{ exp}}$ (mg/g)	equilibrium time (min)	
	VO-OEP	3.23	0.00916	0.996	3.27	1800
	Ni-OEP	3.42	0.00939	0.995	3.46	1800

^aAdsorption temperature: 15 °C; The initial porphyrin concentration: 10 $\mu\text{g/mL}$; The absorbent dosage: $m_{\text{aminated graphene}} = 5 \text{ mg}$, $m_{\text{graphene}} = 5 \text{ mg}$, $m_{\text{VTB-as}^p} = 10 \text{ mg}$.

above, it makes sense that both chemical and physical adsorption existed during the adsorption processes, and the chemical adsorption is seriously inhibited by the aminated side group.

3.5. Function of the Aminated Side Chain. As the structures of asphaltene were very complicated, it is difficult to analyze the functional roles of these structures during the adsorption process. Several model compounds with similar structures to the petroleum asphaltene have been selected as adsorbents to adsorb metal porphyrins. Then, the functional roles of the specified structure could be deduced by comparing the differences of the adsorption behaviors of the adsorbents. In previous study,^{24,25} the differences of adsorption behaviors between VTB-asph and graphene confirmed that the poly aromatic nuclei structure of VTB-asph was the main functional structure for the adsorption of metal porphyrins, while other structures such as heteroatoms, aliphatic side chains, and naphthenic rings may exert negative impact. Now, as N- and O-containing groups were introduced to the poly aromatic nuclei of graphene and caused the structural change, adsorption of metal porphyrins must be affected. Therefore, comparison of adsorption results was conducted to discover the functional role of the aminated and carboxylated side chain during the adsorption of metal porphyrins.

Adsorption results with different adsorbents are shown in Table 10. It can be obviously seen that the equilibrium uptake of metal porphyrins was drastically declined from more than 6 mg/g to about 1 mg/g, after the introduction of the aminated side group to the graphene, which indicated a strong inhibitory effect of the aminated side group for the adsorption of metal porphyrins. It can also be found that adsorption kinetics results with aminated graphene and VTB-asph followed the pseudo-first-order equation, while adsorption kinetics results with graphene followed the pseudo-second-order equation. This illustrates that the internal diffusion of metal porphyrins is the rate-controlling step for aminated graphene and VTB-asph, while the interaction between the adsorbent and adsorbate is the rate-controlling step for graphene. It can be regarded as potential evidence for interpreting why the introduction of the aminated side group inhibited the adsorption of metal porphyrins. Depending on our previous study, the polyaromatic nuclei structure is the main active sites of VTB-asph and graphene for the adsorption of metal porphyrins. It can be concluded that the polyaromatic nuclei structure is also the main active site of the aminated graphene because graphene and aminated graphene have a similar main structure. Therefore, we can assume that there is no significant difference in the interaction between the adsorbate and the three adsorbents. However, the internal diffusion of metal porphyrins for the three processes may have significant differences from each other. First, the graphene could be considered as a two-dimensional material without lateral chains. The steric hindrance effect on the internal diffusion of porphyrins was small, leading to a higher internal diffusion rate, even higher than the surface adsorption rate. Therefore, the adsorbate–adsorbent interaction became the rate-controlling step. On the contrary, for aminated graphene and VTB-asph, their poly aromatic nuclei hydrocarbon skeleton was linked with many lateral chains or groups, which will offer the resistance effect to the internal diffusion. In this case, the internal diffusion rate of metal porphyrins may have declined more severely, even lower than the adsorption rate. Therefore, the internal diffusion step became the rate-controlling step. If

that is the case, it means that the introduction of aminated groups to graphene will cause appreciable steric hindrance to the adsorption process and inhibit the adsorption of metal porphyrins.

Based on the hypothesis above, as a consequence, the adsorption of metal porphyrins on graphene should be faster than that on aminated graphene or VTB-asph, and the adsorption equilibrium time for graphene should also be shorter. According to the experimental results, it was true for VTB-asph. However, for aminated graphene, instead, the results were opposite. In our opinion, the unexpected results could be attributed to the change in the adsorption rate and the number of active sites after the introduction of the aminated group. First, as discussed above, the entire adsorption rate was in connection with the form and number of lateral chains. Compared with VTB-asph, aminated graphene has fewer lateral chains, and the structure of these chains were relatively simple. Therefore, the entire adsorption rate of aminated graphene decreased less than that of VTB-asph. Second, electron delocalization capacity of graphene (Delocalized bonding) was compromised after the introduction of the aminated side group. It may lead to a significant decline of the active sites, which could be confirmed from the decrease in the adsorption capacity (Table 10). Therefore, equilibrium time of aminated graphene was slightly shorter than that of graphene under the joint effect of the decreased active sites and the steric hindrance effect. As for VTB-asph, the internal diffusion rate will be seriously inhibited by its complicated lateral chains. Therefore, it must take longer time to reach the adsorption equilibrium.

More interestingly, the uptake of metal porphyrins of aminated graphene (about 1 mg/g) was much lower than that of VTB-asph (about 3 mg/g). Therefore, except for the poly aromatic nuclei hydrocarbon skeleton and aminated groups, some other structures of asphaltene may exert positive effects on metal porphyrins' adsorption. There are some other results that can be regarded as supplementary evidence to support the conclusion. First, the adsorption isotherms of aminated graphene can be well represented by the Langmuir isotherm model and the adsorption could be considered as a monolayer adsorption. Interactions between metal porphyrins are negligible. However, for VTB-asph, the Freundlich isotherm model is more suitable, and the adsorption could be regarded as multilayer adsorption. It means that there must be other lateral structures that can positively interact with metal porphyrins, transforming the monolayer adsorption to multilayer adsorption and enhancing the adsorption of metal porphyrins. Second, thermodynamics results showed that the absolute values of ΔG° of the adsorption process with aminated graphene were considerably smaller than that with VTB-asph. As a result, adsorption with VTB-asph showed larger spontaneous tendency than that of aminated graphene. There must be other structures which can enhance the interaction between VTB-asph and metal porphyrins, making it stronger than that between aminated graphene and metal porphyrins. Generally, the unit structure model of asphaltene could be simply regarded as a polyaromatic nuclei hydrocarbon skeleton with several heteroatoms (N-, O-, and S-containing groups), aliphatic side chains, and naphthenic rings. The experimental results have confirmed that the carboxyl group (O-containing groups) severely inhibited porphyrins' adsorption. S-containing groups may have similar chemical properties with aminated and carboxyl groups and may similarly inhibit the adsorption.

Therefore, aliphatic side chains and naphthenic rings are more likely to enhance the metal porphyrins' adsorption, which need to be further investigated.

4. CONCLUSIONS

The aminated graphene and carboxylated graphene were used to absorb VO-OEP and Ni-OEP in *n*-pentane solution to investigate the influence of heteroatoms in asphaltene on metal porphyrins' adsorption. Results confirmed that piperazine and carboxyl groups severely inhibited the adsorption. For the latter in particular, the adsorption capacity was almost zero at 25 °C.

The adsorption process with aminated graphene was demonstrated to be a spontaneous, exothermic one. Maximum equilibrium uptake of metal porphyrins was achieved at a higher initial porphyrin concentration and lower temperature and adsorbent dosage. Theoretical simulation results confirmed that the metal porphyrins can be chemically adsorbed on aminated graphene, while the small absolute value of ΔG° calculated from the adsorption thermodynamics study indicated that physical adsorption also contributed to the removal of metal porphyrins. The theoretical simulation results also showed that the physically adsorption loading of metal porphyrins was not evidently affected by the introduction of the aminated side group on graphene, which disagreed with the change of the total adsorption capacity. Therefore, it can be stated that the chemical adsorption was seriously affected by the introduction of the aminated group.

Adsorption results with aminated graphene were compared with graphene and VTB-asp to discover the impact of the aminated side group on the adsorption of metal porphyrins. It was found that the equilibrium uptake of metal porphyrins was significantly declined after the introduction of the aminated side group to graphene. The adsorption kinetics model also changed from the pseudo-second order to the pseudo-first order. We speculate that the introduction of aminated side groups not only compromised the electron delocalization capacity of graphene but also caused a steric hindrance effect on the internal diffusion of metal porphyrins, leading to a decrease of adsorption active sites and internal diffusion rate, respectively.

Equilibrium uptake of metal porphyrins with aminated graphene and carboxylated graphene was found to be even lower than that with VTB-asp. Therefore, aliphatic side chains and naphthenic rings are more likely to enhance the adsorption of metal porphyrins.

AUTHOR INFORMATION

Corresponding Author

Qiushi Zhu – Anhui Province Key Laboratory of Pollutant Sensitive Materials and Environmental Remediation, Huaibei Normal University, Huaibei 235000, P. R. China;
orcid.org/0000-0001-6923-7581;
Phone: +8615155531002; Email: zhu_qs@sina.com

Authors

Feifei Chen – Key Laboratory of Green and Precise Synthetic Chemistry and Applications, Ministry of Education, Huaibei Normal University, Huaibei, Anhui 235000, P. R. China;
orcid.org/0000-0003-4512-1415
Qin Wang – Key Laboratory of Green and Precise Synthetic Chemistry and Applications, Ministry of Education, Huaibei Normal University, Huaibei, Anhui 235000, P. R. China

Linzhou Zhang – State Key Laboratory of Heavy Oil Processing, China University of Petroleum, Beijing 102249, China; orcid.org/0000-0002-8354-784X

Complete contact information is available at:

<https://pubs.acs.org/10.1021/acsomega.2c04811>

Author Contributions

The manuscript was written through contributions of all authors. All authors have given approval to the final version of the manuscript.

Notes

The authors declare no competing financial interest.

ACKNOWLEDGMENTS

This work was supported by the Anhui Provincial Natural Science Foundation [grant No. 1808085QB50], Anhui Peak Disciplines-Chemistry [grant No. GFXK202113], the Open Project of Anhui Province Key Laboratory of Pollutant Sensitive Materials and Environmental Remediation, and Program of Graduate Innovation Research in Huaibei normal university [CX2022043].

REFERENCES

- (1) Wu, J. Y.; Dabros, T. Process for solvent extraction of bitumen from oil sand. *Energy Fuels* **2012**, *26*, 1002–1008.
- (2) Ghosh, A. K.; Chaudhuri, P.; Panja, S. S. Steady state fluorescence spectroscopic studies on the aggregation of coal derived asphaltene at lower concentration. *Fuel* **2016**, *185*, 164–170.
- (3) Zhao, X.; Shi, Q.; Gray, M. R.; Xu, C. New vanadium compounds in venezuela heavy crude oil detected by positive-ion electrospray ionization fourier transform ion cyclotron resonance mass spectrometry. *Sci. Rep.* **2014**, *4*, 5373.
- (4) Liu, H.; Fan, S.; Wang, Z.; Chen, K.; Guo, A. Temperature and pressure effects on the catalytic performance of metalloporphyrins during hydrogenation of naphthalene. *ChemistrySelect* **2017**, *2*, 1613–1619.
- (5) Mousavi, M.; Hosseinneshad, S.; Hung, A. M.; Fini, E. H. Preferential adsorption of nickel porphyrin to resin to increase asphaltene precipitation. *Fuel* **2019**, *236*, 468–479.
- (6) Chen, F.; Liu, Q.; Xu, Z.; Sun, X.; Shi, Q.; Zhao, S. Adsorption kinetics and thermodynamics of vanadyl etioporphyrin on asphaltene in pentane. *Energy Fuels* **2013**, *27*, 6408–6418.
- (7) Castillo, J.; Vargas, V. Metal porphyrin occlusion: adsorption during asphaltene aggregation. *Pet. Sci. Technol.* **2016**, *34*, 873–879.
- (8) Santos Silva, H.; Alfarra, A.; Vallverdu, G.; Bégué, D.; Bouyssiere, B.; Baraille, I. Impact of h-bonds and porphyrins on asphaltene aggregation as revealed by molecular dynamics simulations. *Energy Fuels* **2018**, *32*, 11153–11164.
- (9) Fan, S.; Liu, H.; Wang, J.; Chen, H.; Bai, R.; Guo, A.; Chen, K.; Huang, J.; Wang, Z. Microwave-assisted petroporphyrin release from asphaltene aggregates in polar solvents. *Energy Fuels* **2020**, *34*, 2683–2692.
- (10) Rytting, B. M.; Harper, M. R.; Edmond, K. V.; Zhang, Y.; Kilpatrick, P. K. High-purity vanadyl petroporphyrins: their aggregation and effect on the aggregation of asphaltenes. *Energy Fuels* **2020**, *34*, 164–178.
- (11) Dechaine, G. P.; Gray, M. R. Chemistry and association of vanadium compounds in heavy oil and bitumen, and implications for their selective removal. *Energy Fuels* **2010**, *24*, 2795–2808.
- (12) Filby, R.; Strong, D. Nickel (ii) and vanadium (iv) complexes in alberta oil-sand bitumens. *AIChE Symp. Ser.* **1991**, *87*, 1–9.
- (13) Pernyeszi, T.; Patzkó, A.; Berkesi, O.; Dékány, I. Asphaltene adsorption on clays and crude oil reservoir rocks. *Colloids Surf., A* **1998**, *137*, 373–384.
- (14) Pourmohammadbagher, A.; Shaw, J. M. Probing the impact of asphaltene contamination on kaolinite and illite clay behaviors in

water and organic solvents: a calorimetric study. *Energy Fuels* **2016**, *30*, 6561–6569.

(15) Szymula, M.; Marczewski, A. W. Adsorption of asphaltenes from toluene on typical soils of lublin region. *Appl. Surf. Sci.* **2002**, *196*, 301–311.

(16) Qiang, C.; Gray, M. R.; Qi, L. Irreversible adsorption of asphaltenes on kaolinite: influence of dehydroxylation. *Energy Fuels* **2017**, *31*, 9328–9336.

(17) Abu Tarboush, B. J.; Husein, M. M. Adsorption of asphaltenes from heavy oil onto in situ prepared nio nanoparticles. *J. Colloid Interface Sci.* **2012**, *378*, 64–69.

(18) Pradilla, D.; Subramanian, S.; Simon, S.; Sjöblom, J.; Beurroies, I.; Denoyel, R. Microcalorimetry study of the adsorption of asphaltenes and asphaltene model compounds at the liquid–solid surface. *Langmuir* **2016**, *32*, 7294–7305.

(19) Schuler, B.; Meyer, G.; Peña, D.; Mullins, O. C.; Gross, L. Unraveling the molecular structures of asphaltenes by atomic force microscopy. *J. Am. Chem. Soc.* **2015**, *137*, 9870–9876.

(20) Schuler, B.; Fatayer, S.; Meyer, G.; Rogel, E.; Moir, M.; Zhang, Y.; Harper, M. R.; Pomerantz, A. E.; Bake, K. D.; Witt, M.; et al. Heavy oil based mixtures of different origins and treatments studied by atomic force microscopy. *Energy Fuels* **2017**, *31*, 6856–6861.

(21) González, M. F.; Stull, C. S.; Francisco Lópezlinares, A.; Pereiraalmao, P. Comparing asphaltene adsorption with model heavy molecules over macroporous solid surfaces. *Energy Fuels* **2007**, *21*, 234–241.

(22) Akbarzadeh, K.; Bressler, D. C.; Wang, J.; Gawrys, K. L.; Gray, M. R.; Kilpatrick, P. K.; Yarranton, H. W. Association behavior of pyrene compounds as models for asphaltenes. *Energy Fuels* **2005**, *19*, 1268–1271.

(23) Rakotondradany, F.; Fenniri, H.; Rahimi, P.; Gawrys, K. L.; Kilpatrick, P. K.; Gray, M. R. Hexabenzocoronene model compounds for asphaltene fractions: synthesis & characterization. *Energy Fuels* **2006**, *20*, 2439–2447.

(24) Chen, F.; Zhu, Q.; Xu, Z.; Sun, X.; Zhao, S. Metal porphyrin adsorption onto asphaltene in pentane solution: a comparison between vanadyl and nickel etioporphyrins. *Energy Fuels* **2017**, *31*, 3592–3601.

(25) Chen, F.; Zhu, Q.; Li, S.; Xu, Z.; Sun, X.; Zhao, S. The function of poly aromatic nuclei structure for adsorption of vanadyl/nickel etioporphyrin on asphaltene/graphene. *Fuel Process. Technol.* **2018**, *174*, 132–141.

(26) Mitra-Kirtley, S.; Mullins, O. C.; Van Elp, J.; George, S. J.; Chen, J.; Cramer, S. P. Determination of the nitrogen chemical structures in petroleum asphaltenes using XANES spectroscopy. *J. Am. Chem. Soc.* **1993**, *115*, 252–258.

(27) Moschopedis, S. E.; Speight, J. G. Oxygen functions in asphaltenes. *Fuel* **1976**, *55*, 334–336.

(28) Qian, K.; Mennito, A. S.; Edwards, K. E.; Ferrughelli, D. T. Observation of vanadyl porphyrins and sulfur-containing vanadyl porphyrins in a petroleum asphaltene by atmospheric pressure photonization fourier transform ion cyclotron resonance mass spectrometry. *Rapid Commun. Mass Spectrom.* **2008**, *22*, 2153–2160.

(29) Dechaine, G. P. *Solubility and diffusion of vanadium compounds and asphaltene aggregates*, University of Alberta, 2010, 61–63, doi: DOI: 10.7939/R34P9D.

(30) Hang, Y.; Si, Y.; Zhou, Q.; Yin, H.; Wang, A.; Cao, A. Morphology-controlled synthesis of calcium titanate particles and adsorption kinetics, isotherms, and thermodynamics of cd(ii), pb(ii), and cu(ii) cations. *J. Hazard. Mater.* **2019**, *380*, No. 120789.

(31) Mouni, L.; Belkhir, L.; Bollinger, J.; Bouzaza, A.; Assadi, A.; Tirri, A.; Dahmoune, F.; Madani, K.; Remini, H. Removal of methylene blue from aqueous solutions by adsorption on kaolin: kinetic and equilibrium studies. *Appl. Clay Sci.* **2018**, *153*, 38–45.

(32) Ali, I.; Alharbi, O. M. L.; Alothman, Z. A.; Badjah, A. Y.; Alwarthan, A.; Basheer, A. A. Artificial neural network modelling of amido black dye sorption on iron composite nano material: kinetics and thermodynamics studies. *J. Mol. Liq.* **2018**, *250*, 1–8.

(33) Mahmoud, H. R.; Ibrahim, S. M.; El-Molla, S. A. Textile dye removal from aqueous solutions using cheap MGO nanomaterials: adsorption kinetics, isotherm studies and thermodynamics. *Adv. Powder Technol.* **2016**, *27*, 223–231.

(34) Zarghami, Z.; Akbari, A.; Latifi, A. M.; Amani, M. A. Design of a new integrated chitosan-pamam dendrimer biosorbent for heavy metals removing and study of its adsorption kinetics and thermodynamics. *Bioresour. Technol.* **2016**, *205*, 230–238.

(35) Sabarinathan, C.; Karuppasamy, P.; Vijayakumar, C. T.; Arumuganathan, T. Development of methylene blue removal methodology by adsorption using molecular polyoxometalate: kinetics, thermodynamics and mechanistic study. *Microchem. J.* **2019**, *146*, 315–326.

(36) Ursueguía, D.; Díaz, E.; Ordóñez, S. Adsorption of methane and nitrogen on basolite mofs: equilibrium and kinetic studies. *Microporous. Mesoporous. Mater.* **2020**, *298*, No. 110048.

(37) Schuler, B.; Zhang, Y.; Liu, F.; Pomerantz, A. E.; Andrews, A. B.; Gross, L.; Pauchard, V.; Banerjee, S.; Mullins, O. C. Overview of asphaltene nanostructures and thermodynamic applications. *Energy Fuels* **2020**, *34*, 15082–15105.